Quantifying the role of mechanics in the free and encapsulated growth of cancer spheroids

Stéphane Urcun[1,2,3], Pierre-Yves Rohan[1], Wafa Skalli[1], Pierre Nassoy[4], Stéphane P.A. Bordas[2*], Giuseppe Sciumè[3*]

***For correspondence:** stephane.bordas@alum.northwestern.edu (SPAB); giuseppe.sciume@u-bordeaux.fr (GS)

[1]Institut de Biomécanique Humaine Georges Charpak, Arts et Métiers ParisTech, 151 bd de l'Hôpital, 75013, Paris, France; [2]Institute for Computational Engineering Sciences, Department of Engineering Sciences, Faculté des Sciences, de la Technologie et de Médecine, Université du Luxembourg, Campus Kirchberg, 6, rue Coudenhove-Kalergi, L-1359, Luxembourg.; [3]Institut de Mécanique et d'Ingénierie (I2M), Univ. Bordeaux, CNRS, ENSAM, Bordeaux INP, 33400 Talence, France.; [4]Institut d'Optique Graduate School, CNRS UMR 5298, F-33400 Talence, France.

Abstract Mechanics is of primordial importance to understand cancer; hence, experimental and mathematical models providing quantitative information from the bio-chemo-mechanical perspective play a pivotal role on the development of new therapies. Within this context, encapsulated spheroids are emerging as exceptional *in vitro* tools to investigate the impact of mechanical forces on tumor growth, since from the deformation of the alginate capsule the internal pressure of the spheroid can be retrieved.

We show that multi-phase bio-chemo-poro-mechanics is a suitable theoretical framework to understand, explain and design these *in vitro* tumor growth experiments. Such mechanistic models are based on a set of coupled partial differential equations which are discretized in time and space and solved within an open-source framework (FEniCS). Through sensitivity analyses, our mathematical model suggests that the main parameters determining the encapsulated and free growth configurations are independent. This observation indicates that radically different phenomena are at play during free growth and constrained growth. Our mathematical model, including its open-source implementation and associated sensitivity analysis can help understand important mechanisms in oncophysics through reactive porous media mechanics and serves as a basis for further clinical applications to supplement *in vivo* clinical data.

Introduction

As a tumor grows, it deforms surrounding living tissues, which causes strains and associated stresses. Mechano-biology focuses on the study of interplay between these mechanical forces and biological processes and has been extensively studied experimentally, e.g. (***Helmlinger et al.*** (***1997***)-***Alessandri et al.*** (***2013***)). Mathematical models complement experiments and help understand, explain and build on these experimental findings ***Jain et al.*** (***2014***)(pp.5-6).

Experimental approach

Multi-cellular tumor spheroid (MCTS) cultures have been primarily developed to investigate the complex interactions between cells and the extra-cellular matrix (ECM), such as reactions involving

integrine or the differentiation of epithelial cells, which 2D cultures cannot describe ***Cukierman et al.*** (***2001***). Moreover, the limitation of tissue properties in 2D culture does not allow the evaluation of the efficiency of therapeutic agents on tumor cells ***Alessandri et al.*** (***2013***).
The experiment reproduced here *in silico* is a confined MCTS culture obtained by the adaptation of a patent process of liquid core hydrogel capsules ***Bibette et al.*** (***2012***). Alessandri *et al* ***Alessandri et al.*** (***2013***) developed a microfluidic method based on the encapsulation and growth of cells inside permeable, elastic, hollow microspheres for the production of size-controlled MCTS. Alginate is used as a biomaterial for the encapsulation. Alginates are commonly used for the preservation of transplanted organs and their properties were investigated in ***Lee and Mooney*** (***2012***). Alginate capsules ensure favorable conditions for cellular growth, because its permeability permits the free flow of nutrients and oxygen without requiring additional molecules that could be potentially toxic for the MCTS. By surrounding a growing tumor by an alginate capsule and monitoring the deformation of the capsule, whose mechanical properties can be robustly estimated, it is possible to estimate the forces exerted by the growing tumor on the surrounding capsule. More generally, alginate capsules offer an approach to interrogate, *in vitro*, the interplay between tumor growth and mechanical forces. As measuring strains *in vivo* on tissues is either complex or outright impossible ***Nia et al.*** (***2016***), this reproducible and robust *in vitro* approach is helpful to investigate the pressure exerted by growing tumors onto the surrounding tissues which constrain its growth. These mechanical forces were suggested to contribute to tumor growth regulation ***Helmlinger et al.*** (***1997***), ***Paszek et al.*** (***2005***), hence evaluating their magnitude, distribution and evolution over time could be a key step in devising successful methods to prevent the spread of tumors.
The experiments allow us for monitoring the capsule strains and the MCTS radius during growth. We analysed tumor cell density and evaluated whether the cells are in a proliferating or necrosis state. These experimental results offer invaluable information for the evaluation of any mathematical model for tumor growth.

Modeling approach

The understanding of the physics and mathematical modeling in oncology have made significant progress due to our improved ability to measure physical quantities associated with the development and growth of cancer. These experimental investigations have shown that mechanical stresses influence biology. In particular, it has been shown that such mechanical forces inhibit tumor growth ***Helmlinger et al.*** (***1997***), influence cell differentiation (mechanotransduction) and hence the acquisition of a cancerous phenotype ***Paszek et al.*** (***2005***).
Health research centers have been collaborating with engineers, mathematicians and physicists to introduce mechano-biology within clinical practice. This is particularly true for biochemical and genetic approaches which have been validated on patient cohorts, *e.g.* for the prediction of surgical volume for breast and prostate locations ***Edgerton et al.*** (***2011***), ***Lorenzo et al.*** (***2019***), the prediction of the chemical agent diffusion for pancreatic cancer ***Koay et al.*** (***2014***).
Three physics-based modeling approaches are possible to model cancer: discrete, continuous, hybrid. The reader is referred to more detailed descriptions in the work of ***Lowengrub et al.*** (***2010***). The most advanced continuum models consider tumors as a composite system, fluids and solids, with advection-reaction-diffusion equations for the biochemical part. Furthermore, experimental investigations strongly suggest that tumors are poroelastic solids (***Montel et al.*** (***2011***), ***Douezan and Brochard-Wyart*** (***2012***)). Tumors, as biochemical and biomechanical systems, are multiphasic and heterogeneous: interstitial fluid (IF), nutrient and waste are parts of the cell environment and tumor cells (TC) are included in the ECM network. Poromechanics emerges today as one valid approach to model and simulate the interplay between biomechanical and biochemical phenomena. The mathematical model employed here is based on the original approach designed in ***Sciumè et al.*** (***2013***), enriched in ***Sciumè et al.*** (***2014c***) by a multiphase fluid constitutive relationship and further generalized in ***Sciumè et al.*** (***2014a***) to account for deformation of the extracellular matrix. This tumor growth modeling approach is a subset of a more general set of methods within the

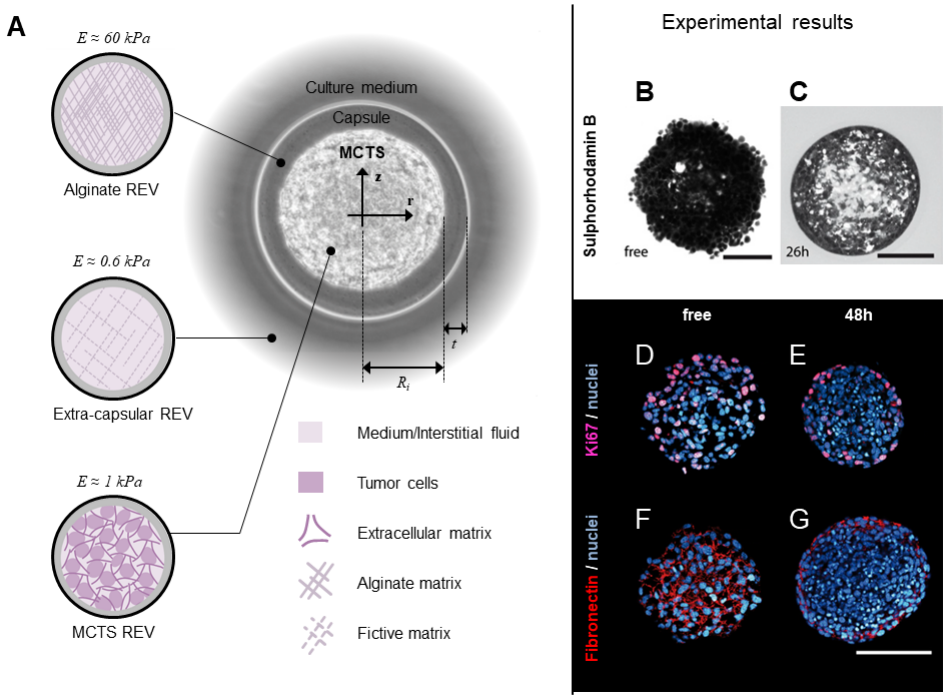

Figure 1. The capsule model. **A** Geometrical description of the capsule and assumed representative elementary volumes (REV): Three spatial domains modeled within the same mathematical framework: MCTS REV (consisting of tumor cells, IF and extracellular matrix), the alginate shell (only IF phase within a solid scaffold of Young Modulus $E = 60$Kpa) and extra-capsular domain (only IF phase within a fictive solid scaffold of Young Modulus $E = 0.6$Kpa) enforced by the theoretical framework. **B**-**G** From ***Alessandri et al.*** (***2013***), imaging of the internal cellular organization of growing spheroids under elastic confinement. Snapshots taken by two-photon imaging of free (**B**) and encapsulated (**C**) spheroids stained with the polar dye SRB are shown. Time t = 0 corresponds to confluence. Co-focal images of free (**D** and **F**) and confined (**E** and **G**) spheroids after cryosection and immunolabeling for DAPI, KI67 (magenta), fibronectin (red), and cell nucleus (blue). (Scale bars: **B**–**C**, 50 μm; **D**, **E**, **F**, and **G**, 100 μm.)

theory of porous media and was also used to describe ulceration and necrosis of human plantar tissues, for patient with diabetes ***Sciumè et al.*** (***2014b***).

In this article, we specialize this reference model to numerically reproduce the experiment of ***Alessandri et al.*** (***2013***) gaining additional information not yet measurable *in vitro*.

Methods and Model

The presented experimental results are based on Cellular Capsule Technology (CCT, Alessandri *et al*. ***Alessandri et al.*** (***2013***)). CCT offers an ideal framework to quantitatively assess the impact of mechanical stresses and its coupling with other biophysical factors which impact tumor cells proliferation and metabolism. Unknowns of the mathematical model can in fact be retrieved from the CCT experimental data. This motivated the selection of CCT as reference experimental The CCT experiment, the mathematical model and the computational framework developed are described in the following paragraphs.

Growth of encapsulated MCTS: experimental procedure and observed phenomenology

In this reference experiment ***Alessandri et al.*** (***2013***) MCTS is cultured within an alginate spherical capsule, a few hundreds of microns in diameter. These alginate capsules are built using a microfluidic co-extrusion device: the outer sheath is made of a sodium alginate solution; an intermediate compartment contains a calcium-free medium; and the inner core is composed of the

cell suspension (CT26 mouse colon carcinoma). Performing extrusion in the air, the liquid jet is fragmented into droplets (due to Plateau-Rayleigh instability) which upon contact with a calcium bath, readily crosslink as shells encapsulating cells (alginate undergoes gelation in the presence of divalent ions). The capsule allows convection of interstitial fluid (IF) and diffusion of nutrients species, growth factors and drugs through its surface; however, thanks to alginate pores' size (of the order of 20 nm), cells cannot escape. The capsule therefore serves as micro-compartment for the 3D cell culture. During growth, the tumor deforms its surroundings which reacts with a confinement pressure. The mechanism is similar to what happens in the CCT experiment: during cell proliferation, the fraction of capsule volume occupied by cells increases until the capsule is filled (confluence); then the tumor spheroid starts to strongly interact with the capsule and deforms it. After confluence, the alginate capsule, deformed by the MCTS, responds with a confinement pressure due to action-reaction principle. This confinement pressure and non-optimal oxygenation of the MTCS core areas generate important measurable heterogeneities (necrosis, local increase in cell density, etc.) along the spheroid radius.

CCT allows generating capsules with desired size and shell thickness. This can be achieved by regulation of extrusion velocity and suitable geometrical adjustment of the co-extrusion device (see ***Alessandri et al.*** (***2013***) for more details). To test the reliability of the mathematical model we considered two capsule classes: 1) a first set of capsules having an external radius of around 100μm and a shell thickness of around 30μm designed as *"thick capsules"*; 2) a second set of capsules with the same mean external radius of the thick capsules but a shell thickness of around 10μm, these are designed as *"thin capsules"*. A third set of non-encapsulated MCTS (with the same cell line) has been used as control. Results for non-encapsulated MCTS growth are designed as *"free MCTS"* in the follow.

Before confluence, in both thick and thin capsules, the growth rate of the CT26 spheroid is almost the same as that of the free MCTS case, indicating that access to nutrients is not compromised by the presence of the alginate shell. After confluence, the behavior strongly deviates from that of the free MCTS case. In the previous article ***Alessandri et al.*** (***2013***), we observed qualitatively the same phenomenology in thick and thin capsules. However results are quantitatively very different due to the different overall stiffness of the alginate capsules. We monitored the evolution of MCTS radius, capsule strain and cells states (proliferating or not) over several days. Images were taken at regular intervals by time-lapse phase-contrast microscopy (***Figure 1***D-G). MCTS volumes were computed from the measured radii, assuming a spherical geometry. To label the necrotic core of the tumor, we used sulforhodamine B (SRB) with two-photon microscopy (***Figure 1***B,C). The proliferating cells were examined using Ki-67 staining (***Figure 1***D,E). We observed that the proliferating cells were uniformly distributed in the free growing MCTS ***Figure 1***D) while after confluence, in the encapsulated MCTS, cell division principally occurred in the peripheral rim (***Figure 1***E).

Regarding the dilatation of the alginate capsule, we characterized it as an elastic deformation with negligible plasticity and no hysteresis. Young's modulus was measured by atomic force microscopy indentation and osmotic swelling, giving a range of 68 ± 21kPa ***Alessandri et al.*** (***2013***). Thanks to the identified Young's modulus, capsules can be used as a biophysical dynamometer as a relation can be constructed which relates the variation of the inner pressure with radial deformation, monitored using video-microscopy.

The pressure exerted by the MCTS is calculated using the formalism of thick-walled internally pressurized spherical vessels.

Assuming that the alginate gel is isotropic and incompressible the radial displacement of the inner wall, $u(R_{\text{in}})$, reads

$$u(R_{\text{in}}) = \frac{3}{4}\frac{P}{E}\frac{R_{\text{in}}}{1-(R_{\text{in}}/R_{\text{out}})^3}.$$

where P is the internal pressure, E is the Young's modulus, and R_{in} and R_{out} are the inner and outer radii of the capsule, respectively. Alginate incompressibility also implies volume conservation of

the shell. This gives the following constraint equation

$$R^3_{\text{out}}(t) - R^3_{\text{in}}(t) = R^3_{\text{out}}(0) - R^3_{\text{in}}(0) = \delta(R^3_0).$$

Using this equation, the two time variables $R_{\text{in}}(t)$ and $R_{\text{out}}(t)$ can be separated and pressure, $P(t)$, written as a function of $R_{\text{in}}(t)$ only

$$P(t) = \frac{4}{3}E\left[1 - \frac{1}{1+\delta(R^3_0)/R^3_{\text{in}}(t)}\right]\frac{u(R_{\text{in}}(t))}{R_{\text{in}}(t)}.$$

Experimentally, we thus need to measure only the initial outer and inner radii and track the evolution either the inner radius of the capsule.

The mathematical model: a physics-based description of the MCTS-capsule system

The mathematical model is governed by momentum and mass conservation equations of phases and species constituting the MCTS-capsule system. Once the capsule is formed, three different spatial domains can be defined (***Figure 1***A): the intra-capsular domain where the tumor cells phase (t), the medium/interstitial fluid phase (l) and the extra-cellular matrix phase (s) coexist ; the alginate shell domain, where a solid scaffold phase (s) and the medium fluid phase (l) coexist; and the extra-capsular domain where the only medium fluid phase (l) exist. The three domains are explicitly modeled mathematically by an extension of the TCAT-based multiphase modeling framework proposed by Sciumè *et al.* in ***Sciumè et al.*** (***2014a***). Our approach considers the tumor tissue as a reactive porous multiphase system: tissue extra-cellular matrix constitutes the solid scaffold while interstitial fluid (IF) and tumor cells (TC) are modeled as fluid phases. Strains are calculated according to the theory of poro-elasticity which always assumes the presence of a certain solid phase volume fraction which constitutes the porous/fibrous medium. Therefore, a certain proportion of the solid phase must always be present even where it does not exist in the real system (*e.g.* in the extra-capsular domain). Despite this unrealistic condition enforced by the theoretical framework, the reliability of the model is only weakly affected, because the stiffness of this fictitious solid phase is two orders of magnitude lower than that of the alginate solid scaffold (***Figure 1***A). A unique physical model is defined for the three domains, with some penalty parameters (*e.g.* a low intrinsic permeability) avoiding cell infiltration in the alginate shell domain. Oxygen advection-diffusion within the medium/interstitial fluid phase, l, is also considered.
Starting from the general form of conservation equations provided by TCAT in ***Gray and Miller*** (***2014***), the final system of governing equations is obtained. It consists of four equations:

- the t phase mass conservation
- the l phase mass conservation
- the advection-diffusion equation of oxygen in the l phase
- the momentum conservation equation of the multiphase system

We have four primary variables: three are scalar, namely the pressure of the medium/interstitial fluid, p^l, the pressure difference between the cell phase t and the medium/interstitial fluid l, p^{tl}, the mass fraction of oxygen, $\omega^{\bar{n}l}$; one is vectorial, the displacement of the solid scaffold, $\mathbf{u}^s$. We have two internal variables: the porosity ε and the TC necrotic fraction ω^{Nt}.
We introduce two kinds of closure relationships for the system: mechanical and mechano-biological. Details about derivation of the governing equations and this constitutive relationships are provided in appendix Appendix A. The Multiphase System.
The parameters of these closure relationships are of critical importance and will be studied through a detailed sensitivity analysis. First, a saturation-pression relationship depending on two variables, p^{tl} and ω^{Nt}, and a constant parameter, a the ECM network thinness: $S^l(p^{tl}, \omega^{Nt}, a)$. Its detailed description could be found in Appendix A. The Multiphase System, eq.20 and ***Figure 7***. Second, the TC growth rate and TC nutrient consumption function which are dependent on both oxygen and

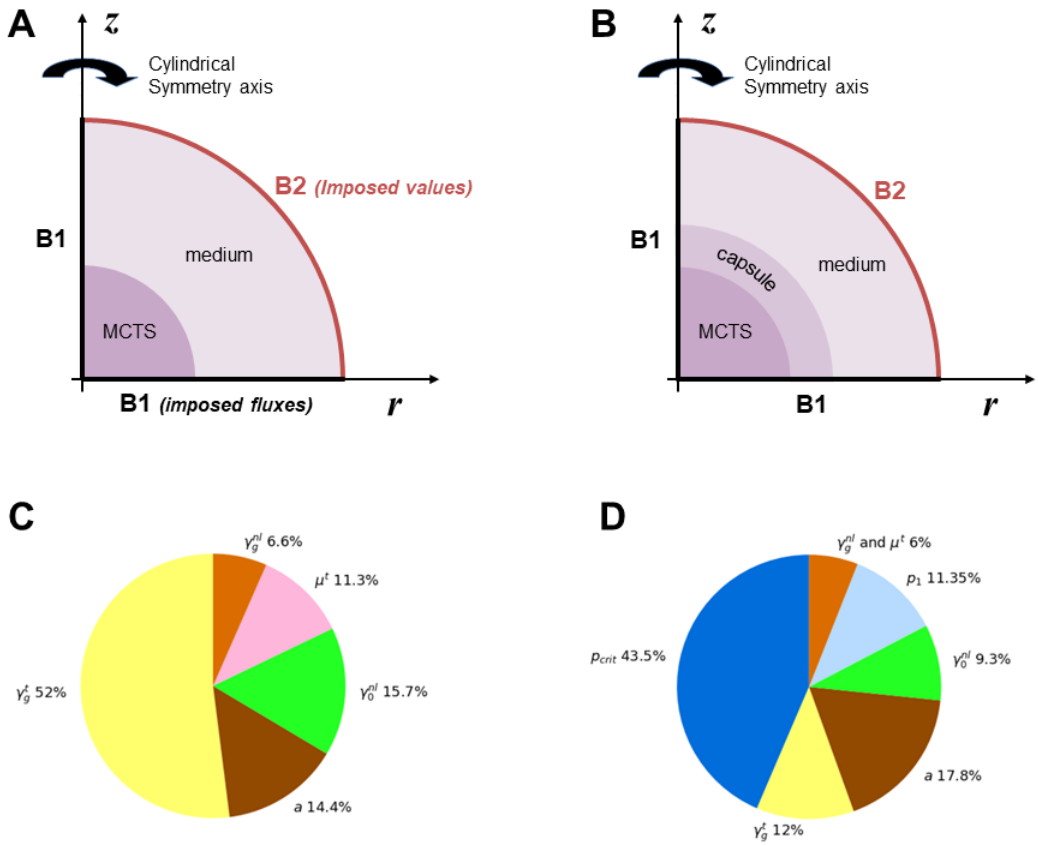

Figure 2. Modeling and sensitivity of free and encapsulated MCTS. **A** Free MCTS configuration, with the following boundary conditions: B1 no normal fluxes, B2 Dirichlet condition $\mathbf{u}^s = \vec{0}$, $p^l = 0$, $p^{tl} = 0$ and $\omega^{\bar{n}l} = 4.2e^{-6}$. **B** Encapsulated MCTS, in a capsule of radius R and thickness t, with the same boundary conditions than the free MCTS. **C** Weighted FE solution sensitivity to the 7 parameters of the model for the free MCTS configuration. Only 5 parameters remain, the governing parameter is γ_g^t, the tumor cells growth rate, the sensitivity solution to the pressure parameters, p_1 and p_{crit}, is 0. **D** Weighted FE solution sensitivity to the 7 parameters of the model for the encapsulated MCTS configuration. The governing parameter is p_{crit} the inhibitory pressure of tumor cells growth.

pressure level through two tuples of parameters: (ω_{env}, ω_{crit}) and (p_1, p_{crit}). They define threshold functions which govern activation or inhibition of the biological processes, for further information please see Appendix A. The Multiphase System, eq.22, 23 and ***Figure 8***.

The cell phase consists of living and necrotic species. Even if the model does not explicitly discriminate between proliferative and quiescent cells, the TC growth is subject to the above parameters. To make possible the comparison with the experimental proliferative cell quantities, we set a TC proliferative fraction dependent on the mass fraction $\omega^{\bar{n}l}$ (Appendix A. The Multiphase System, eq.26).

Computational framework

We implemented the above model in Python and C++ within the FEniCS framework ***Alnæs et al.*** (***2015***), with an incremental monolithic resolution of the mixed finite element (FE) formulation and assuming cylindrical symmetry. The simulations have been run with composite Taylor-Hood element $P_3(\mathbb{R}^2)$, $[P_2(\mathbb{R})]^3$ (one vectorial and three scalar unknowns), a mesh cell size of $dh = 5\mu$m and an implicit Euler scheme with $dt = 1200$ s. An updated lagrangian approach is adopted to account for geometrical nonlinearity. All the details and analytical verification of the FE formulation can be

found in Appendix B. Computational framework.

For all the sensitivity or optimization topics, we measured the error by the root mean square error (RMSE) relatively to a reference, specified each time. The error on the numerical quantity ξ_{num} relative to a reference ξ_{ex}, evaluated at n points is:

$$RMSE(\xi_{\text{num}}, \xi_{\text{ex}}, n) = \sqrt{\frac{1}{n}\sum_{k=1}^{n}\left(\frac{\xi_{\text{ex}}(k) - \xi_{\text{num}}(k)}{\xi_{\text{ex}}(k)}\right)^2}$$

Presentation of the two configurations

Figure 2 shows the two modeled configurations of MCTS. We assumed cylindrical symmetry in the simulations: each mesh is a half of a sphere, because we also exploit symmetry with respect to a diametrical plane.

For the three scalar variables, we prescribed Dirichlet boundary conditions along the outer radius of the domain $p^l = 0$, $p^{tl} = 0$, $\omega^{\bar{n}l} = 4.2e^{-6}$ [1] and no flux condition at $r = 0$ and $z = 0$. For the ECM displacement field $\mathbf{u}^s$, slip conditions $u_r^s = 0|_{r=0}$ and $u_z^s = 0|_{z=0}$ are used, and Dirichlet conditions $\mathbf{u}^s = \mathbf{0}$ at the outer radius of the domain (see ***Figure 2***).

In ***Alessandri et al.*** (***2013***), the free configuration is used as a classical control group and it is a useful tool for simulation too. The same cell line, CT26 mouse colon carcinoma, being used for both free and encapsulated configuration, it allows us to test the same parameters set in two very different physical conditions.

In-silico reproduction process

The experimental input data were, for the free MCTS, the volume monitored over a time span of 12 days and several images of cell nucleus in a proliferating state; for the encapsulated MCTS, the aggregate volume, the capsule strain monitored for 8 days and the imaging of cell nuclei. We chose a reference case of a capsule of inner radius $= 100\mu$m and thickness $= 34\mu$m.

We performed a detailed sensitivity study of the FE solution on the parameters, both on the free and encapsulated MCTS. The seven parameters of the model have been set to generic values, gathered in Table Parameters for the CT26 cell line. We took those values from ***Chignola et al.*** (***2000***) and ***Sciumè et al.*** (***2014a***), they were already used in other *in silico* studies (***Mascheroni et al.*** (***2016***), ***Santagiuliana et al.*** (***2019***)). The FE solutions with these values have been compared with the experimental results, at day 4 for the free MCTS and day 1 (after confluence) for the encapsulated MTCS. This gave us the generic error named costs J_{free} and J_{conf} respectively. To perform the sensitivity analysis, we have chosen the following design of experiment (DOE): each parameter, one at a time, have been perturbed of $[-10, -5, -2, -1, +1, +2, +5, +10]\%$ for each configuration and the corresponding cost has been computed. All the details of the process, auxiliary parameters and cost functions can be found in Appendix C. Sensitivity analysis.

The optimization has been based on sensitivity profiles and the parameters have been identified by the Nelder-Mead simplex algorithm for both configurations. Parameters were identified with an alginate capsule of stiffness $E = 68$ kPa, the mean experimental value.

To evaluate the identified parameters, an author of this article and member of the team of ***Alessandri et al.*** (***2013***) has provided unpublished experimental results of encapsulated MCTS, both thick and thin. As their alginate stiffness was not known (the Young's modulus of the alginate was estimated as $E = 68 \pm 21$ kPa), two simulations have been run for each capsule with the extreme values of E. This provided to us the range of modeling possibilities of the optimized parameters.

The following model outputs have been compared to the experimental results: volume, capsule strain, TC density and necrotic fraction.

[1] which corresponds, according to Henry's law, to 90mmHg, the usual oxygen mass fraction in arteries (see ***Ortiz-Prado et al.*** (***2019***))

Table 1. Parameters for the CT26 cell line

Parameter	Symb.	Generic	Unit	Source	Optimized
ECM network thinness	a	800	Pa	Initial guess	890
Dynamic viscosity of TC	μ_t	36	Pa.s	***Sciumè et al.*** (***2014a***)	
TC growth rate	γ_g^t	4.10^{-2}	kg/(m^3.s)	***Chignola et al.*** (***2000***)	$3.33.10^{-2}$
TC growth O_2 consump.	γ_g^{nl}	4.10^{-4}	kg/(m^3.s)	***Chignola et al.*** (***2000***)	
TC metabolism O_2 consump.	γ_0^{nl}	6.10^{-4}	kg/(m^3.s)	***Chignola et al.*** (***2000***)	$6.65.10^{-4}$
Start TC growth inhibitory	p_1	1800	Pa	Initial guess	1432
Stop TC growth	p_{crit}	4000	Pa	Initial guess	5944

Results

Based on a detailed sensitivity study, the optimized set of parameters was tested and crossvalidated on unpublished experimental results provided by the same team of ***Alessandri et al.*** (***2013***). Numerical simulation also provides a wide output of qualitative results (*e.g.* IF flux, necrotic fraction and TC saturation, etc.) which are presented and interpreted at the end of the section.

Sensitivity analysis

The second line of ***Figure 2*** summarizes the results of DOE. We have obtained two distinct profiles of sensitivity for the two configurations. The parameters associated with each of the two configurations can thus be identified separately.

For the free MCTS configuration, the governing parameter is γ_g^t the tumor cells growth rate (weighted, 52%). For all parameters perturbations of the DOE, the pressure of the TC phase $p^t = p^l + p^{tl}$ is lesser than 1 KPa, thus the first threshold of growth inhibitory due to pressure p_1 is never reached and, *a fortiori*, the critical threshold of total inhibition p_{crit}. For the whole DOE of the free configuration, the sensitivity of the FE solution to p_1 and p_{crit} is 0. Thus, only five parameters remain and only three gather 82.1% of the cost function variation: γ_g^t, γ_0^{nl} the oxygen rate consumption due to metabolism (15.7%) and a the ECM network thickness coefficient (14.4%).

For the encapsulated configuration, the most important parameter is the critical inhibitory pressure p_{crit} (43.5%). Only two parameters gather 54.9% of the cost function variation: p_{crit} and p_1 (11.35%).

Optimization

We identified the three governing parameters $\gamma_g^t, \gamma_0^{nl}, a$ for the free MCTS configuration by the Nelder-Mead simplex algorithm and fitted to the experimental data with a $RMSE = 0.031$. To be physically relevant, the same parameters set should be shared by the two configurations, thus we have injected these three parameters within the encapsulated configuration and we identified its two governing parameters p_1, p_{crit} by the same algorithm. We fit the experimental data of the encapsulation with a $RMSE = 0.124$. ***Figure 3***A shows the two configurations fitted with the following set of parameters: $\gamma_g^t = 3.33.10^{-2}$, $\gamma_0^{nl} = 6.65.10^{-4}$, $a = 890$, $p_1 = 1432$, $p_{\text{crit}} = 5944$ (see Table 1). This set is cell-line specific, only relevant for CT26 mouse colon carcinoma. Eight days after confluence, we note that the results are obtained with a tumor cells pressure $p^t < p_{\text{crit}}$, in accordance with the experiment as recorded in ***Alessandri et al.*** (***2013***) the MCTS continues to growth twelve days after confluence, even very slowly. Thus, this total growth inhibition threshold can be interpreted as an *asymptotic* growth inhibition.

Validation

Unpublished experimental results of encapsulated MCTS, both thick and thin, has been used to validate the optimized set. Each capsule has its own radius R and thickness t and two simulations have been run with the extreme experimental values of the alginate stiffness ($E = 47$kPa and

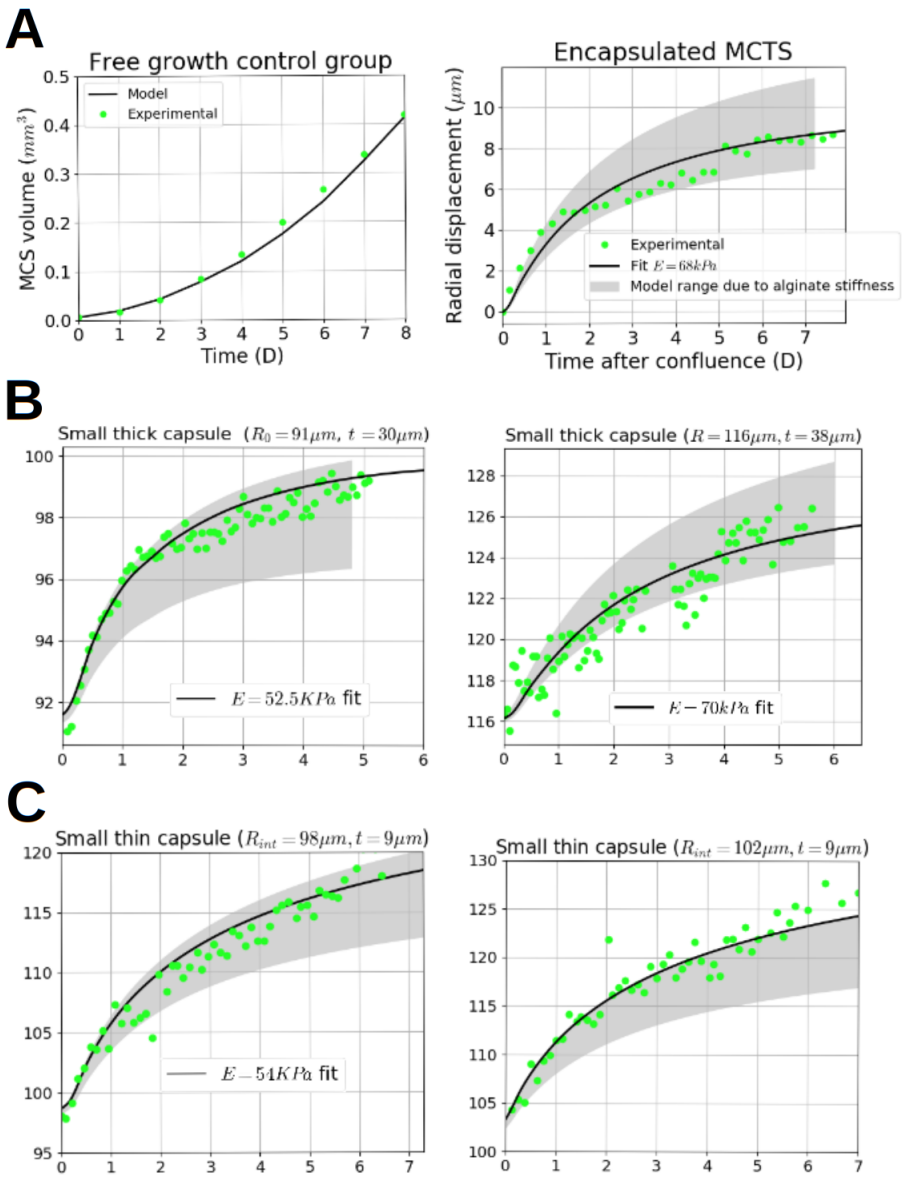

Figure 3. Validation of the optimized parameters. Alginate Young's estimated in ***Alessandri et al.*** (***2013***) as $E = 68 \pm 21$ kPa. Simulations with the extreme values of E give the range of modeling possibilities of the optimized set. Experimental results, green dotted ; Numerical results with the optimized parameters set, black; Modeling range, grey filled. **A**, free MCTS control group, Time (Day) versus MCTS volume (mm^3); encapsulated MCTS configuration, Time (Day) versus radial displacement (μm). Fit with $E = 68$kPa. **B** Validation of the identified parameters on 2 thick capsules. Time (Day) versus Capsule radius (μm). The experimental points are in the modeling range. Both capsule fit with $E = 52.5$kPa and $E = 70$kPa respectively. **C** Partial validation of the identified parameters on 2 thin capsules. Time (Day) versus Capsule radius (μm). Left, one capsule is fitted with $E = 54$kPa ; right, the experimental points are at the boundary of the modeling range.

$E = 89$kPa). ***Figure 3***A shows the range of modeling possibilities of the optimized parameters, respectively to the alginate stiffness range. ***Figure 3***B shows the validation on 2 thick capsules with an alginate stiffness at $E = 52.5$kPa and $E = 70$kPa respectively. The modeling range is in accordance with these experimental results. ***Figure 3***C shows validation on one thin capsule and the other is fitted with the lower stiffness value $E = 47$kPa, as the linear elastic hypothesis applied to alginate is limited assumption for this level of deformation ($> 20\%$). However, we showed that the model could adapt to different geometries without lost its relevance: ***Figure 3***B left and ***Figure 3***C left show, with the same parameters set and almost the same alginate stiffness ($E_{B,\text{Left}} = 52.5$kPa and $E_{C,\text{Left}} = 54$kPa), the model reproducing experimental deformation of 8 and 16%, the difference being a purely geometrical effect due to the capsule thickness.

Qualitative results and physical interpretation

Beyond overall quantitative results, ***Figure 4*** and ***Figure 5*** provide details on the physical phenomena occurring during growth (from confluence to 85 hours after confluence) of a MTCS encapsulated in a thick capsule with an initial internal radius of almost 100 μm. These figures allow to quickly understand the importance of physics-based modeling, as it provides qualitative information that could be used to interpret the experiment process as a whole and to better understand the tumor growth process. ***Figure 4*** shows contours of oxygen, necrotic fraction, IF pressure, ECM displacement, TC pressure and TC saturation at confluence and 85 hours after. To gain information about the dynamics of these quantities, ***Figure 5*** shows them probed along the radius at confluence, 85 hours after, and at two intermediate times (28 and 56 hours).

Figure 5A and B show the interplay between oxygen consumption and necrosis. Indeed as mentioned in the experiments, 85 hours after confluence, the viable space remaining for TC is a $20\,\mu$m thick rim. This is explicit in ***Figure 4***, upper right circle, NTC quarter. ***Figure 5***C shows the IF pressure evolution, after confluence, we see a sucking phenomenon due to IF absorption by growing TC. As the cells activity decrease at the MCTS inner core, IF accumulates and its pressure becomes positive during a certain time (see ***Figure 5***C, 28h). After confluence the initial gradient of IF pressure (green line in ***Figure 5***C) inverses sense: cells in the proliferative peripheral areas move toward the core so IF has to go in the opposite direction (due to mass conservation). After 2 days of quick growth, experimentally and numerically, the MTCS reaches a state of linear and slow evolution and from that point onwards, the IF flux will not qualitatively change. This overall dynamic is clearly visible on ***Figure 5***D and E, as the capsule displacement is driven by TC partial pressure. The comparison of ***Figure 5***F and B show a relation between the saturation of TC and their necrotic fraction. This is a basic experimental fact that, when the cells bodies collapse in a necrotic core, the aggregate density increase accordingly.

We reproduce another case presented in ***Alessandri et al.*** (***2013***) to study the quantitative level of TC saturation and necrotic fraction in a $50\,\mu$m radius capsule. ***Figure 6***A and ***Figure 6***B present cell densities, proliferative and necrotic, ***Figure 6***A for a free MCTS of 50μm radius and ***Figure 6***B for a MCTS in a 50μm radius alginate capsule, 26 hours after confluence. The same CT26 cell-line specific parameters have been used within this geometry and the results are compared with the free MCTS simulation at the same radius, see ***Figure 6***C and D, respectively. Both configurations show a very good agreement with the experimental results.

Discussion

We show in this paper how an experimental/computational approach can help to quantify the relative importance of physical phenomena involved in growth of cancerous tumors. Our proof-of-concept application is founded on an *in vitro* physical model where an MTCS grows within an alginate spherical capsule. This experiment is based on a well established protocol that allows us to tune the capsule stiffness and estimate by inverse analysis the pressure inside the spheroid

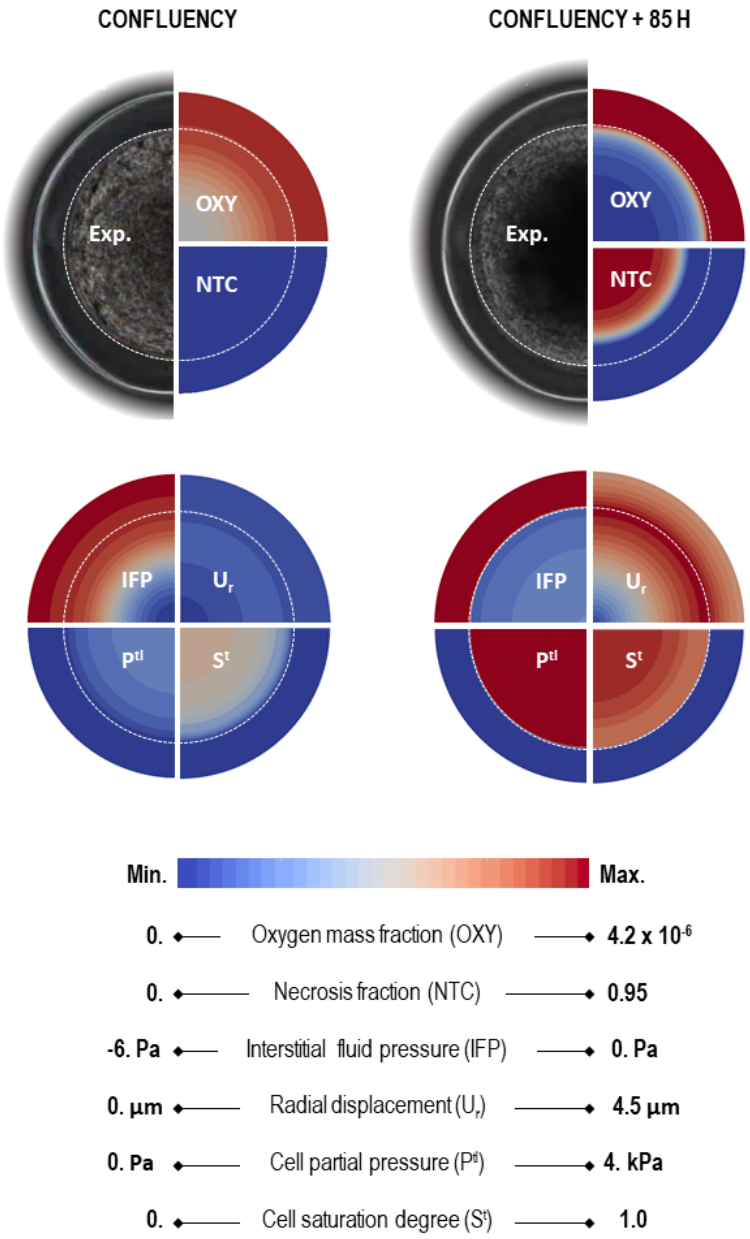

Figure 4. Qualitative results, experimental and 6 physical quantities from the modeling: oxygen, necrotic tumor cells, interstitial fluid pressure, radial displacement, partial tumor cells pressure and tumor cells saturation. Left, at confluence. Right, 85 hours after confluence. The mass of growing tumor cells is directly taken to interstitial fluid, this implies a sucking phenomenon at the inner capsule radius (down right, upper left quarter). According to the experiment, a 20 μm thick viable rim is obtain 85 hours after confluence (upper right, right half), the tumor cell saturation depends both on partial pressure and necrotic fraction (down right, down right quarter).

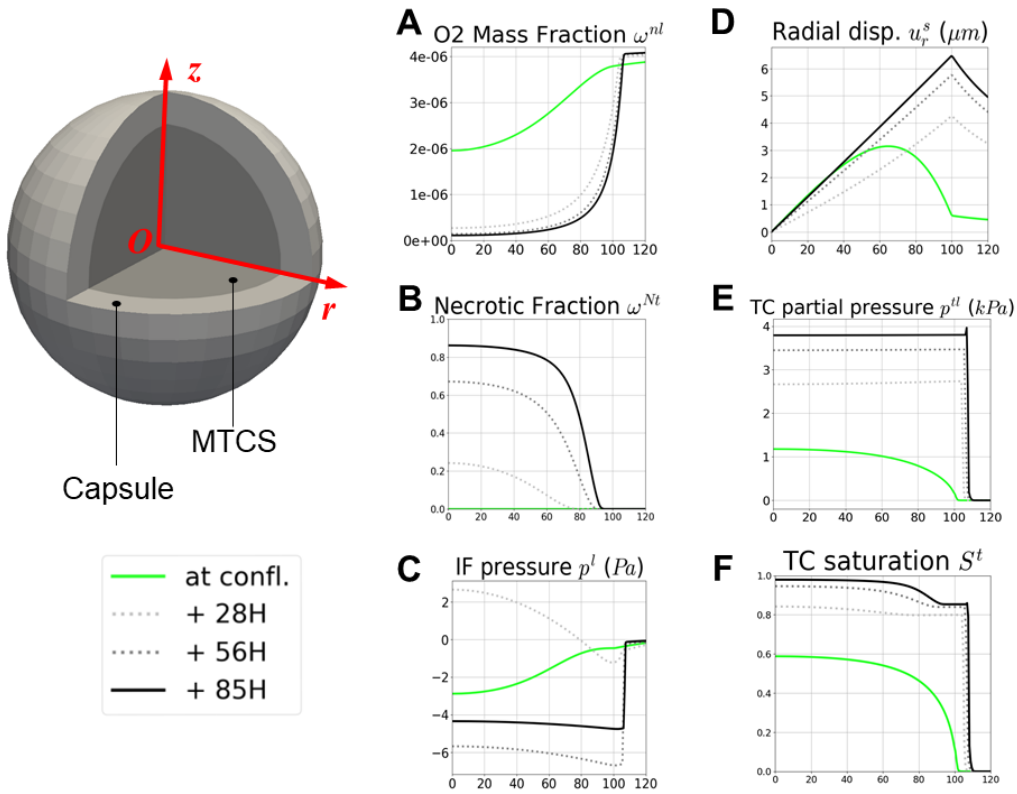

Figure 5. Quantities probed along the $r = z$ line at confluence, 85 hours after, and two intermediate times (28 and 56 hours): **A** oxygen, **B** necrotic fraction, **C** IF pressure, **D** ECM displacement, **E** TC pressure and **F** TC saturation. **A** and **B**: as mentioned in the experiments, 85 hours after confluence the viable space remaining for TC is a $20\,\mu$m thick rim. **C**: after confluence, IF is absorbed by growing TC, provoking a sucking phenomenon, as the cells activity decrease at the MCTS inner core, IF accumulates and its pressure becomes positive. As described in ***Alessandri et al.*** (***2013***), after 2 days of quick growth, the MTCS reaches a state of linear and slow evolution. **D** and **E**: the capsule displacement is driven by TC pressure with the same overall dynamic. **E**, **F** and **B**: relation between the saturation of TC and their necrotic fraction, the TC aggregate density increases with necrotic core.

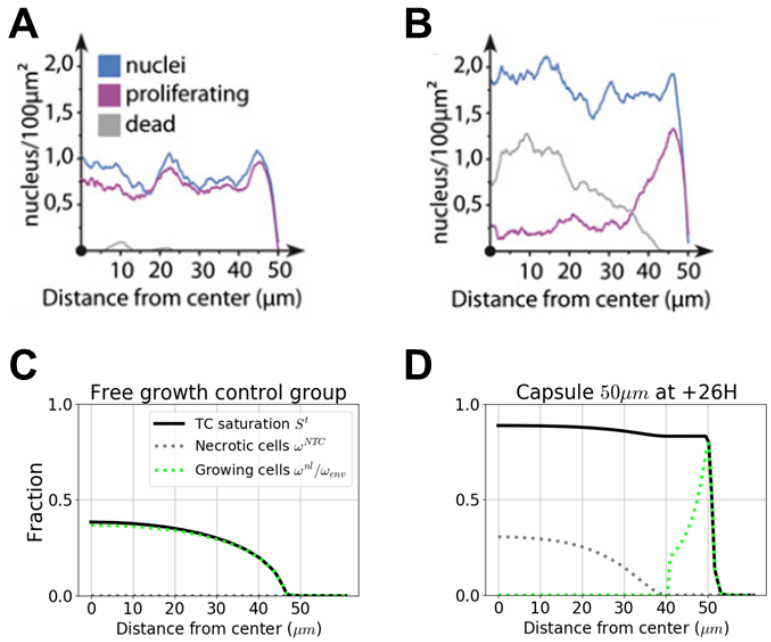

Figure 6. Quantification of proliferating and dead cells radial densities for free and confined CT26 spheroids: *in vitro-in silico* results. Experimental quantification of cell nuclei (blue), proliferating cells (purple),and dead cells (gray) along the radius for free, **A**, and confined, **B**, growth. Numerical results for 3 fractional quantities (TC Saturation S^t, black, Necrotic saturation of TC $\omega^{Nt}S^t$, gray dotted, Growing TC fraction $\omega^{TC}_{\text{grow}}$, green dotted) vs distance from center in free, **C**, and encapsulated, **D**, configuration. TC saturation almost doubles between the two configurations, in encapsulation, necrotic fraction occupy almost half of the TC phase and only a thin rim of the MTCS is viable.

Alessandri et al. (***2013***). Such experiment has been simulated *in silico* by means of an bio-chemo-mechanical mathematical model theoretically founded on mechanics of reactive porous media. If we compare such model with the phase-field model proposed by some of us in ***Le Maout et al.*** (***2020***), the proposed *porous medium* formulation results more suitable for simulation of the *post*-confluence behavior since deformation of the capsule and geometrical non-linearity is accounted explicitly. The phase-field approach is conversely more reliable to model the *prior to*-confluence behavior and growth within other geometries where the MCTS is not fully in contact with the alginate shell ***Le Maout et al.*** (***2020***).

The sensitivity analysis we performed shows that the parameters which govern the growth in free and encapsulated conditions are almost independent, which suggests the physical phenomena should be independent too.

After identification of the parameters, the same parameter set fits both the free and encapsulated MCTS in a thick capsule ($R = 100\mu$m, $t = 34\mu$m) (***Figure 3***A). To ensure that the identification process is robust, we crossvalidated it on other genuine thick capsule experiments ($R = 91\mu$m, $t = 30\mu$m) and ($R = 116\mu$m, $t = 38\mu$m) (***Figure 3***B). For thin capsules, despite the trends of the obtained numerical solutions are good, our results indicate that the linear elastic hypothesis adopted for alginates is not suitable when the strain regime is relatively large (***Figure 3***C). The rich output of the mathematical model provides information about phenomena not yet observable or quantifiable *in vitro* (see ***Figure 4***) and allows for quantification of living and necrotic cells along the capsule radius (***Figure 6***).

This poromechanical approach offers a unified framework to model both the growing MTCS and the alginate capsule accounting mechanistically for their mechanical interaction. This makes such approach well-suited to help interpretation and further improvement of experiments presented in this paper. Mechano-biological coupling allows us to reproduce the dynamics of growth and

hypoxia of both free and encapsulated MCTS and to retrieve the strain of the biomaterial. We show that cross-validation of the model (on a set of different cases) and sensitivity analyses allow enhancing the synergy between *in silico* an *in vitro* modeling. When cross-validation leads to a non-exhaustive agreement between numerical and experimental results this is indicative of a non-proper constitutive relationship (or starting hypothesis) that is identified and adjusted or fully modified. Following a deductive scientific methodology, we have systematically tested the mathematical model not trying to validate it but conversely trying to highlight its limitations. This has allowed to progressively improve it and finally to achieve a predictive (non- phenomenological) formulation.

In 2020s mathematical modeling in oncology begins to enter a stage of maturity; today mathematical models of tumor growth tend to clinical applications and therefore must be really predictive and funded on measurable or at least quantifiable parameters having, as much as possible, a sound physical meaning. This motivated this paper which presents not only a mechanistic bio-chemo-poromechanical model but also a *modus procedendi* to achieve a certain predicative potential and, with intercession of sensitivity analysis, to quantify relative relevance of mechanisms underlying tumor growth phenomenology.

Acknowledgments

The authors acknowledge ENSAM *Réseau Santé* (health institutional network), fondation Arts et Métiers and University of Luxembourg that have financially supported the project as well as the funding of the University of Luxembourg, of the DRIVEN H2020 TWINNING Project 2020driven.uni.lu

References

Alessandri K, Sarangi BR, Gurchenkov VV, Sinha B, Kießling TR, Fetler L, Rico F, Scheuring S, Lamaze C, Simon A, Geraldo S, Vignjević D, Doméjean H, Rolland L, Funfak A, Bibette J, Bremond N, Nassoy P. Cellular capsules as a tool for multicellular spheroid production and for investigating the mechanics of tumor progression in vitro. Proceedings of the National Academy of Sciences. 2013; 110(37):14843–14848. https://www.pnas.org/content/110/37/14843.

Alnæs M, Blechta J, Hake J, Johansson A, Kehlet B, Logg A, Richardson C, Ring J, Rognes M, Wells G. The FEniCS Project Version 1.5. Archive of Numerical Software. 2015; 3(100). http://journals.ub.uni-heidelberg.de/index.php/ans/article/view/20553.

Bibette J, Chu L, Carreras E, Royere A, N B. Method for Manufacturing Capsule Series, and Related Capsule Series, US patent publication 2012/0003285. . 2012; .

Boffi D, Brezzi F, Fortin M. Mixed Finite Element Methods and Applications. Springer; 2013.

Chignola R, Schenetti A, Andrighetto G, Chiesa E, Foroni R, Sartoris S, Tridente G, Liberati D. Forecasting the growth of multicell tumour spheroids: implications for the dynamic growth of solid tumours. Cell Proliferation. 2000; 33(4):219–229. https://onlinelibrary.wiley.com/doi/abs/10.1046/j.1365-2184.2000.00174.x.

Cukierman E, Pankov R, Stevens DR, Yamada KM. Taking Cell-Matrix Adhesions to the Third Dimension. Science. 2001; 294(5547):1708–1712. https://science.sciencemag.org/content/294/5547/1708.

Douezan S, Brochard-Wyart F. Dewetting of cellular monolayers. Eur Phys J E. 2012; 35(5):34. https://doi.org/10.1140/epje/i2012-12034-9.

Edgerton ME, Chuang YL, Macklin P, Yang W, Bearer EL, Cristini V. A Novel, Patient-Specific Mathematical Pathology Approach for Assessment of Surgical Volume: Application to Ductal Carcinoma *in situ* of The Breast. Analytical Cellular Pathology. 2011; 34.

Gray WG, Miller CT. Introduction to the Thermodynamically Constrained Averaging Theory for Porous Medium Systems. Springer; 2014.

Helmlinger G, Netti PA, Lichtenbeld HC, Melder RJ, Jain RK. Solid stress inhibits the growth of multicellular tumor spheroids. Nature Biotechnology. 1997; 15(21):778–783.

Jain RK, Martin JD, Stylianopoulos T. The Role of Mechanical Forces in Tumor Growth and Therapy. Annual Review of Biomedical Engineering. 2014; 16(1):321–346. https://doi.org/10.1146/annurev-bioeng-071813-105259.

Khan N, Williams BB, Hou H, Li H, Swartz HM. Repetitive tissue pO2 measurements by electron paramagnetic resonance oximetry: current status and future potential for experimental and clinical studies. Antioxidants & redox signaling. 2007; 9(8):1169–1182.

Koay EJ, Truty MJ, Cristini V, Thomas RM, Chen R, Chatterjee D, Kang Y, Bhosale PR, Tamm EP, Crane CH, Javle M, Katz MH, Gottumukkala VN, Rozner MA, Shen H, Lee JE, Wang H, Chen Y, Plunkett W, Abbruzzese JL, et al. Transport properties of pancreatic cancer describe gemcitabine delivery and response. The Journal of clinical investigation. 2014; 124(4):1525–1536.

Le Maout V, Alessandri K, Gurchenkov B, Bertin H, Nassoy P, Sciumè G. Role of mechanical cues and hypoxia on the growth of tumor cells in strong and weak confinement: A dual in vitro–in silico approach. Science Advances. 2020; 6.

Lee KY, Mooney DJ. Alginate: properties and biomedical applications. Progress in polymer science. 2012; 37(1):106–126.

Lorenzo G, Hughes TJR, Dominguez-Frojan P, Reali A, Gomez H. Computer simulations suggest that prostate enlargement due to benign prostatic hyperplasia mechanically impedes prostate cancer growth. Proceedings of the National Academy of Sciences. 2019; 116(4):1152–1161. https://www.pnas.org/content/116/4/1152.

Lowengrub JS, Frieboes HB, Jin F, Chuang YL, Li X, Macklin P, Wise SM, Cristini V. Nonlinear modelling of cancer: bridging the gap between cells and tumours. Nonlinearity. 2010; 23(1).

Mascheroni P, Stigliano C, Carfagna M, Boso DP, Preziosi L, Decuzzi P, Schrefler BA. Predicting the growth of glioblastoma multiforme spheroids using a multiphase porous media model. Biomechanics and Modeling in Mechanobiology. 2016; 15(1):1215–1228.

Montel F, Delarue M, Elgeti J, Malaquin L, Basan M, Risler T, Cabane B, Vignjevic D, Prost J, Cappello G, Joanny JFmc. Stress Clamp Experiments on Multicellular Tumor Spheroids. Phys Rev Lett. 2011 Oct; 107:188102. https://link.aps.org/doi/10.1103/PhysRevLett.107.188102.

Nia HT, Liu H, Seano G, Datta M, Jones D, Rahbari N, Incio J, Chauhan VP, Jung K, Martin JD, Askoxylakis V, Padera TP, Fukumura D, Boucher Y, Hornicek FJ, Grodzinsky AJ, Baish JW, Munn LL, Jain RK. Solid stress and elastic energy as measures of tumour mechanopathology. Nature Biomedical Engineering. 2016; 1.

Ortiz-Prado E, Dunn JF, Vasconez J, Castillo D, Viscor G, Warner F, Zucker SW. Partial pressure of oxygen in the human body: a general review. American journal of blood research. 2019; 9(1):1–14.

Paszek MJ, Zahir N, Johnson KR, Lakins JN, Rozenberg GI, Gefen A, Reinhart-King CA, Margulies SS, Dembo M, Boettiger D, Hammer DA, Weaver VM. Tensional homeostasis and the malignant phenotype. Cancer cell. 2005; 8:241–254.

Santagiuliana R, Milosevic M, Milicevic B, Sciumè G, Simic V, Ziemys A, Kojic M, Schrefler BA. Coupling tumor growth and bio distribution models. Biomedical microdevices. 2019; 21.

Sciumè G, Gray WG, Hussain F, Ferrari M, Decuzzi P, Schrefler BA. Three phase flow dynamics in tumor growth. Computational Mechanics. 2014c; 53(3):465–484.

Sciumè G, Santagiuliana R, Ferrari M, Decuzzi P, Schrefler BA. A tumor growth model with deformable ECM. Physical biology. 2014a; 11(6).

Sciumè G, Shelton S, Gray WG, Miller CT, Hussain F, Ferrari M, Decuzzi P, Schrefler BA. A multiphase model for three-dimensional tumor growth. New Journal of Physics. 2013 jan; 15(1):015005. https://doi.org/10.1088/1367-2630/15/1/015005.

Sciumè G, Boso DP, Gray WG, Cobelli C, Schrefler BA. A two-phase model of plantar tissue: a step toward prediction of diabetic foot ulceration. International Journal for Numerical Methods in Biomedical Engineering. 2014b; 30(11):1153–1169. https://onlinelibrary.wiley.com/doi/abs/10.1002/cnm.2650.

Stein E, de Borst R, Hughes TJR. Encyclopedia of Computational Mechanics, Vol. 1. Wiley; 2017.

Verruijt A. Theory and Problems of Poroelasticity; 2013. https://geo.verruijt.net/.

Appendix A. The Multiphase System

We give in this section all the details about governing equations and the constitutive relationships. According to the different phases, solid scaffold s, medium/interstitial fluid l and tumor cells phase t, described in the main article, section Methods, which constitute the multiphase system, at each point in the domain, the following constraint must be respected

$$\varepsilon^s + \varepsilon^t + \varepsilon^l = 1, \tag{1}$$

where ε^α is the volume fraction of phase α. Defining the porosity ε as

$$\varepsilon = 1 - \varepsilon^s, \tag{2}$$

Equation 1 can also be expressed in terms of the saturation degree of the fluid phase, $S^f = \varepsilon^f/\varepsilon$ (with $f = t, l$)

$$S^t + S^l = 1. \tag{3}$$

Mass conservation equations

We express the mass conservation equation for each phase. We use a material description for the motion of the solid phase and a spatial description for the fluid phases, whose reference space is that occupied by the solid scaffold. As the solid is deformable, this reference space is not fixed in time but evolves according to the displacement of the solid phase. For this reason we express mass conservation equations for each phase and species in their material form with respect to the solid scaffold velocity. Mass conservation equations of solid, cell and interstitial fluid phases read:

$$\frac{D^s}{Dt}(\rho^s\varepsilon^s) + \rho^s\varepsilon^s\nabla\cdot\mathbf{v}^{\bar{s}} = 0, \tag{4}$$

$$\frac{D^s}{Dt}\left(\rho^t\varepsilon S^t\right) + \nabla\cdot(\rho^t\varepsilon S^t\mathbf{v}^{\bar{ts}}) + \rho^t\varepsilon S^t\nabla\cdot\mathbf{v}^{\bar{s}} = \sum_{i\in l}\overset{il\to t}{M}, \tag{5}$$

$$\frac{D^s}{Dt}\left(\rho^l\varepsilon S^l\right) + \nabla\cdot(\rho^l\varepsilon S^l\mathbf{v}^{\bar{ls}}) + \rho^l\varepsilon S^l\nabla\cdot\mathbf{v}^{\bar{s}} = -\sum_{i\in l}\overset{il\to t}{M}, \tag{6}$$

where $\frac{D^s}{Dt}$ is the material time derivative with respect to the solid phase, ρ^α is the density of phase α, $\mathbf{v}^{\bar{s}}$ is the velocity vector of the solid phase, $\sum_{i\in l}\overset{il\to t}{M}$ is the total mass exchange (water, oxygen and other nutrients) from the interstitial fluid to the tumor due to cell growth and metabolism, $\mathbf{v}^{\bar{ts}}$ is the relative velocity of cells, and $\mathbf{v}^{\bar{ls}}$ is relative velocity of the interstitial fluid.
The tumor cell phase is a mixture of living (LTC) and necrotic tumor cells (NTC), with mass fraction $\omega^{\bar{L}t}$ and $\omega^{\bar{N}t}$, respectively. The following constraint applies

$$\omega^{\bar{L}t} + \omega^{\bar{N}t} = 1. \tag{7}$$

Mass conservation equations for each fraction, assuming that there is no diffusion of both necrotic and living cells, read

$$\frac{D^s}{Dt}\left(\rho^t\omega^{\bar{L}t}\varepsilon S^t\right) + \nabla\cdot(\rho^t\omega^{\bar{L}t}\varepsilon S^t\mathbf{v}^{\bar{ts}}) + \rho^t\omega^{\bar{L}t}\varepsilon S^t\nabla\cdot\mathbf{v}^{\bar{s}} = \sum_{i\in l}\overset{il\to t}{M} - \varepsilon^t r^{Nt}, \tag{8}$$

$$\frac{D^s}{Dt}\left(\rho^t\omega^{\bar{N}t}\varepsilon S^t\right) + \nabla\cdot(\rho^t\omega^{\bar{N}t}\varepsilon S^t\mathbf{v}^{\bar{ts}}) + \rho^t\omega^{\bar{N}t}\varepsilon S^t\nabla\cdot\mathbf{v}^{\bar{s}} = \varepsilon^t r^{Nt}, \tag{9}$$

where $\varepsilon^t r^{Nt}$ is the death rate of tumor cells. Note that only one of Eqs 8-9 is independent: actually, one can be obtained subtracting the other from Eqn 5 and accounting for the constraint Eqn 7.
Oxygen is the only nutrient which we consider explicitly. Another mass balance equation is introduced which governs the advection-diffusion of oxygen, n, within the interstitial fluid

$$\frac{D^s}{Dt}\left(\rho^l\omega^{\bar{n}l}\varepsilon S^l\right) + \nabla\cdot(\rho^l\omega^{\bar{n}l}\varepsilon S^l\mathbf{v}^{\bar{ls}}) + \nabla\cdot(\rho^l\omega^{\bar{n}l}\varepsilon S^l\mathbf{u}^{\bar{n}l}) + \rho^l\omega^{\bar{n}l}\varepsilon S^l\nabla\cdot\mathbf{v}^{\bar{s}} = -\overset{nl\to t}{M}, \tag{10}$$

where $\mathbf{u}^{\bar{nl}}$ is the diffusive velocity of oxygen in the interstitial fluid and $\overset{nl\to t}{M}$ the oxygen consumed by tumor cells due to their metabolism and proliferation rate.

Momentum conservation equations

We neglect here the effect of gravitational body forces as their contribution is negligible compared to that of other forces. Furthermore, as we assume quasi-static processes and small difference in density between cells and aqueous solutions, inertial forces and the force due to mass exchange can also be neglected. These assumptions simplify the general form of the linear momentum balance equation given in ***Gray and Miller*** (***2014***) which becomes

$$\nabla \cdot (\varepsilon^{\alpha}\mathbf{t}^{\bar{\bar{\alpha}}}) + \sum_{K\in\mathfrak{J}_{c\alpha}} \overset{K\to\alpha}{\mathbf{T}} = \mathbf{0} \quad (\alpha = s,t,l), \tag{11}$$

where $\mathbf{t}^{\bar{\bar{\alpha}}}$ is the stress tensor of phase α, $\mathfrak{J}_{c\alpha}$ is the set phases connected to α and $\overset{K\to\alpha}{\mathbf{T}}$ is the interaction force between phase α and the adjacent phases. Summing eqn 11 over all phases gives the momentum equation of the whole multiphase system as

$$\nabla \cdot \mathbf{t}^{\bar{\bar{T}}} = \mathbf{0}, \tag{12}$$

where $\mathbf{t}^{\bar{\bar{T}}}$ is the total Cauchy stress tensor acting on the multiphase system.
Assuming that for relatively slow flow, the stress tensor for a fluid phase, f, can be properly approximated as

$$\mathbf{t}^{\bar{\bar{f}}} = -p^f\mathbf{1} \quad (f = t,l) \tag{13}$$

where p^f is the averaged fluid pressure and $\mathbf{1}$ the unit tensor, Eqn. 11 which apply for a generic phase α (solid or fluid) can be expressed in an alternative form for fluid phases as ***Sciumè et al.*** (***2013***)

$$\varepsilon^f\nabla p^f + \mathbf{R}^f \cdot (\mathbf{v}^{\bar{f}} - \mathbf{v}^{\bar{s}}) = \mathbf{0} \quad (f = t,l) \tag{14}$$

where $\mathbf{R}^f$ is a symmetric second order resistance tensor accounting for interaction between the fluid phase and the solid phase, s. Eqn. 14 can be rewritten as

$$-\mathbf{K}^f \cdot \nabla p^f = \varepsilon^f(\mathbf{v}^{\bar{f}} - \mathbf{v}^{\bar{s}}) \quad (f = t,l), \tag{15}$$

where $\mathbf{K}^f = (\varepsilon^f)^2(\mathbf{R}^f)^{-1}$ is called the hydraulic conductivity. The hydraulic conductivity depends on the dynamic viscosity of the flowing fluid, μ^f, on the intrinsic permeability of the porous scaffold, k, and on the fluid saturation degree, S^f, via a relative permeability function $k^f_{\text{rel}}(S^f)$. As customary in biphasic flow problems we set here $\mathbf{K}^f = k\frac{k^f_{\text{rel}}(S^f)}{\mu^f}\mathbf{1}$. Hence, the governing linear momentum conservation equations for tumor cells and interstitial fluid read

$$-k\frac{k^t_{\text{rel}}(S^t)}{\mu^t}\nabla p^t = \varepsilon^t(\mathbf{v}^{\bar{t}} - \mathbf{v}^{\bar{s}}), \tag{16}$$

$$-k\frac{k^l_{\text{rel}}(S^l)}{\mu^l}\nabla p^l = \varepsilon^l(\mathbf{v}^{\bar{l}} - \mathbf{v}^{\bar{s}}), \tag{17}$$

Effective stress principle and closure relationships

We assume here that fluid phases are incompressible and the solid phase is almost incompressible. However, the overall multiphase system is not incompressible, because of the presence of porosity that evolves according with the scaffold deformation. As phases are incompressible, their densities ρ^{α} with $\alpha = s,t,l$ are constant. As the solid phase is quasi incompressible, the Biot's coefficient is set to unity. With these premises, the total Cauchy stress tensor appearing in eqn 12 is related to the Biot's effective stress as follows

$$\mathbf{t}^{\bar{\bar{E}}} = \mathbf{t}^{\bar{\bar{T}}} + p^s\mathbf{1}, \tag{18}$$

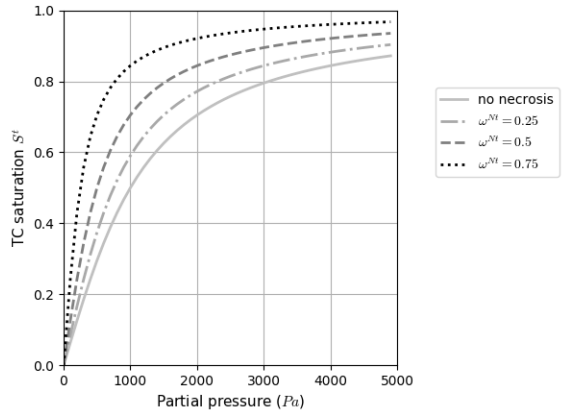

Appendix 0 Figure 7. Tumor cell phase saturation S^t, with the parameter a fixed to 1kPa, evolving with the necrotic fraction of the phase $\omega^{\tilde{N}t}$

where $p^s = S^t p^t + S^l p^l$ is the so-called solid pressure, describing the interaction between the two fluids and the solid scaffold.

The chosen closure relationship for the effective stress $\mathbf{t}^{\bar{\bar{E}}}$ is linear elastic:

$$\mathbf{t}^{\bar{\bar{E}}} = \bar{\bar{\bar{\bar{C}}}} : \epsilon(\mathbf{u}^{\bar{s}}), \tag{19}$$

with $\epsilon(u^s) = \frac{1}{2}(\nabla \mathbf{u}^{\bar{s}} + (\nabla \mathbf{u}^{\bar{s}})^T)$ and $\bar{\bar{\bar{\bar{C}}}}(E, \nu)$ the fourth order elasticity tensor depending on E the Young modulus of the solid scaffold and ν its Poisson ratio.

The experimental measurement of cells density inside the capsule revealed a strong dependency to necrotic fraction $\omega^{\tilde{N}t}$. Hence, the pressure-saturation closure relationship has been improved with respect to that proposed in ***Sciumè et al.*** (***2014b***), to be more physically relevant and adapted to confinement situation

$$S^t = \frac{2}{\pi} \arctan\left(\frac{p^{tl}}{(1 - \omega^{\tilde{N}t})a}\right), \tag{20}$$

with p^{tl} pressure difference between tumor and interstitial fluid (i.e. $p^{tl} = p^t - p^l$). The saturation is directly linked to the partial pressure of the phase and a constant parameter a, which represents refinement of the porous/fibrous network. Its influence is offset by the necrotic fraction of tumor cells, $\omega^{\tilde{N}t}$ (see Fig.***Figure 7***), which allows us to model necrotic areas of very high cell density according with experimental evidence.

Fick's law is adopted to model diffusive flow of oxygen.

Tumor cells growth, metabolism and necrosis

$\sum_{i \in l} \overset{il \to t}{M}$, the total mass exchange from interstitial fluid to the tumor cell phase is defined as

$$\sum_{i \in l} \overset{il \to t}{M} = \gamma_g^t \mathcal{H}(\omega^{\tilde{nl}}) \left(1 - \mathcal{H}_p(p^t)\right) \left(1 - \omega^{\tilde{N}t}\right) \varepsilon S^t, \tag{21}$$

with γ_g^t the tumor growth rate parameter, cell-line dependent. $\mathcal{H}$ and $\mathcal{H}_p$ are regularized step functions varying between 0 and 1, with two threshold parameters σ_1, σ_2: $\mathcal{H} = \mathcal{H}(\sigma, \sigma_1, \sigma_2)$. When the variable σ is greater than σ_2, $\mathcal{H}$ is equal to 1, it decreases progressively when the variable is between σ_1 and σ_2 and is zero when the variable is lower that σ_1. $\mathcal{H}$ represent the growth dependency to

oxygen:

$$\mathcal{H}(\omega^{\bar{nl}}, \omega_{\text{crit}}, \omega_{\text{env}}) = \begin{cases} 0 \quad \text{if} \quad \omega^{\bar{nl}} \leq \omega_{\text{crit}} \\ \\ \frac{1}{2} - \frac{1}{2}\cos\pi\frac{\omega^{\bar{nl}} - \omega_{\text{crit}}}{\omega_{\text{env}} - \omega_{\text{crit}}} \quad \text{if} \quad \omega_{\text{crit}} \leq \omega^{\bar{nl}} \leq \omega_{\text{env}} \\ \\ 1 \quad \text{if} \quad \omega^{\bar{nl}} \geq \omega_{\text{env}} \end{cases} \tag{22}$$

ω_{env}, the optimal oxygen mass fraction, is set to $4,2.10^{-6}$ which corresponds, according to Henry's law, to 90mmHg, the usual oxygen mass fraction in arteries (see ***Ortiz-Prado et al.*** (***2019***)). ω_{crit}, the hypoxia threshold, is cell-line dependent, for tumor cells, it has been set to a very low value: 10^{-6} ($\approx$ 20mmHg, for common human tissue cells, hypoxic level is defined between 10 and 20mmHg ***Khan et al.*** (***2007***)) The function $\mathcal{H}(\omega^{\bar{nl}}, \omega_{\text{crit}}, \omega_{\text{env}})$ is plotted ***Figure 8***A.

Function $(1 - \mathcal{H}_p)$ represents the dependency on pressure:

$$\mathcal{H}_p(p^t, p_1, p_{\text{crit}}) = \begin{cases} 0 \quad \text{if} \quad p^t \leq p_1 \\ \\ \sqrt{\frac{p^t - p_1}{p_{\text{crit}} - p_1}} \quad \text{if} \quad p_1 \leq p^t \leq p_{\text{crit}} \\ \\ 1 \quad \text{if} \quad p^t \geq p_{\text{crit}} \end{cases} \tag{23}$$

We set p_{crit} to 6kPa as initial guess (in ***Helmlinger et al.*** (***1997***), they found a inhibitory pressure at 10kPa) and p_1, the pressure threshold when the inhibitory process starts, at 2kPa. The function $\mathcal{H}_p(p^t, p_1, p_{\text{crit}})$ is plotted ***Figure 8***B.

The tumor oxygen consumption $\overset{nl\to t}{M}$ follows the law

$$\overset{nl\to t}{M} = \left[\gamma_g^{nl}\mathcal{H}(\omega^{\bar{nl}})\left(1 - \mathcal{H}_p(p^t)\right) + \gamma_0^{nl}\tilde{\mathcal{H}}\right](1 - \omega^{\bar{N}t})\varepsilon S^t, \tag{24}$$

with γ_g^{nl} the consumption rate due to proliferation, γ_0^{nl} the consumption rate due to quiescent metabolism and $\tilde{\mathcal{H}}$:

$$\tilde{\mathcal{H}}(\omega^{\bar{nl}}) = \begin{cases} 1 \quad \text{if} \quad \omega^{\bar{nl}} \geq \omega_{\text{crit}} \\ \\ \frac{1}{2} - \frac{1}{2}\cos\pi\frac{\omega^{\bar{nl}}}{\omega_{\text{crit}}} \quad \text{else} \end{cases} \tag{25}$$

The model does not discriminate between proliferating and quiescent cells, but the growth is subject to $\mathcal{H}(\omega^{\bar{nl}}, \omega_{\text{crit}}, \omega_{\text{env}})$. To make possible the comparison with the experimental proliferative cell quantities, the following relationship has been set:

$$\omega_{\text{grow}}^{TC} = \begin{cases} 0 \quad \text{if} \quad \omega^{\bar{nl}} \leq \omega_{\text{crit}} \\ \\ S^t\frac{\omega^{\bar{nl}}}{\omega_{\text{env}}} \quad \text{else} \end{cases} \tag{26}$$

$\tilde{\mathcal{H}}$ is also used in the definition of hypoxic necrosis rate which reads

$$\varepsilon S^t r^{Nt} = \gamma^{Nt}(1 - \tilde{\mathcal{H}}(\omega^{\bar{nl}}))(1 - \omega^{\bar{N}t})\varepsilon S^t, \tag{27}$$

where $\gamma^{Nt} = 0.01$ is the necrotic growth rate. Its value has not been changed in this article.

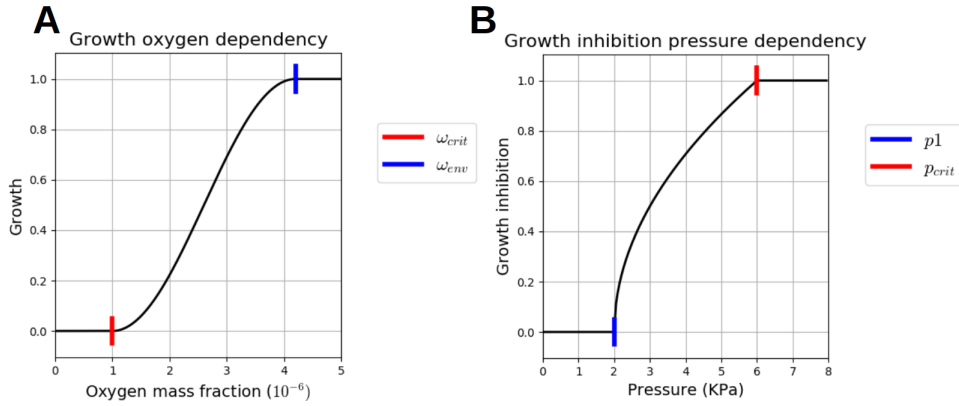

Appendix 0 Figure 8. Two mechano-biological laws. **A** $\mathcal{H}(\omega^{\bar{nl}}, \omega_{\text{env}}, \omega_{\text{crit}})$. The TC growth and nutrient consumption are dependent to the oxygen mass fraction $\omega^{\bar{nl}}$. If it is lower than ω_{crit}, the TC growth is stopped and the nutrient consumption is reduced to the metabolism needs only. If it is greater or equal to ω_{env}, the growth and the nutrient consumption are maximum. **B** $\mathcal{H}_p(p^t, p_{\text{crit}}, p_1)$. The TC growth and nutrient consumption are dependent to the TC pressure. If it is greater than p_1, the 2 processes begin to be strongly affected and if the TC pressure reaches p_{crit}, they are totally stopped.

Appendix B. Computational framework

The model has been coded in Python and C++ in the open-source FEniCS framework ***Alnæs et al.*** (***2015***) with an incremental monolithic resolution of the mixed finite element (FE) formulation, under a cylindrical axis symmetry hypothesis, and a fully implicit Euler scheme in time. The incremental resolution allows us to update primary variables as follows:

$$\mathbf{X}_{n+1} = \mathbf{X}_n + \delta\mathbf{X} \tag{28}$$

with $\delta\mathbf{X}$ the vector of unknowns

$$\delta\mathbf{X} = \begin{pmatrix} \delta u_r^s \\ \delta u_z^s \\ \delta p^l \\ \delta p^{tl} \\ \delta\omega^{\bar{nl}} \end{pmatrix}$$

After each time step, the space $\mathcal{X}^s \in \mathbb{R}^2$ is updated:

$$\mathcal{X}_{n+1}^s = \mathcal{X}_n^s + \delta\mathbf{u}^s$$

All the codes used in this article, analytical verification, free growth and confined growth, are available on Github, at https://github.com/StephaneUrcun/MCTS_mechanics

Choice of the element

For all mixed FE problem with vectorial and scalar coupled unknowns, the chosen finite element should verify the inf-sup condition, that is to say, should preserve the coercivity of the bilinear form (see ***Boffi et al.*** (***2013***) p.223-230). A simple choice is the Taylor-Hood element, with a Lagrange element of order $k \geq 1$ for the scalar unknowns and order $k+1$ for the vectorial one. However, modelling an encapsulated tumor growth implies a very sharp gradient at the capsule inner radius for the partial pressure of the tumor cells phase p^{tl}. The linear approximation of the Lagrange element of order 1 could not describe it, except at the cost of an extremely refined mesh at the interface, and the error could provoke *numerical infiltration* of tumor cells in the alginate capsule (see Fig.***Figure 9***). To avoid this phenomenon, the composite Taylor-Hood element has been set to a higher order, precisely the mixed FE formulation in FEniCS uses the composite Taylor-Hood element $P_3(\mathbb{R}^2), [P_2(\mathbb{R})]^3$. The demonstration of Lax-Milgram theorem for this type of mixed problem could be found in the *Encyclopedia of Computational Mechanics*, Vol.1, p.149-202 ***Stein et al.*** (***2017***).

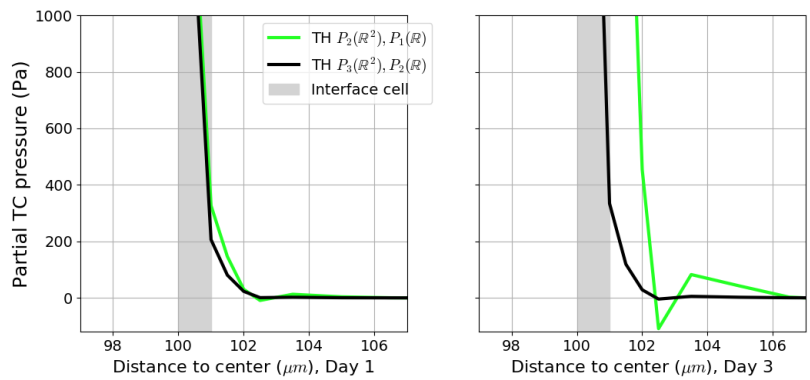

Appendix 0 Figure 9. Choice of the element (composite Taylor-Hood $P_2(\mathbb{R}^2), [P_1(\mathbb{R})]^3$, green ; composite Taylor-Hood $P_3(\mathbb{R}^2), [P_2(\mathbb{R})]^3$, brown). The linear approximation $P_1(\mathbb{R})$ of the partial tumor cells pressure at the capsule interface (Interface element shared, black) is poor (Left, Day 1) and provoke numerical infiltration of tumor cells into the alginate capsule (Right, Day 3)

Appendix 0 Table 2. Relative degradation of the solution due to mesh cell size. Measured by root mean square, the reference being the thinner mesh with a cell size of $dh = 2.5\,\mu$m.

	$dh = 50\,\mu$m	$dh = 20\,\mu$m	$dh = 10\,\mu$m	$dh = 5\,\mu$m
$RMSE(dh, 2.5\,\mu\text{m}, 400/dh)$	0.182	0.032	0.019	0.010

Choice of the mesh cell size

The mixed FE problem has been computed on 5 different meshes, with uniform cell sizes $dh = 50, 20, 10, 5$ and 2.5μm. To measure the FE solution degradation the primary variable $\omega^{\vec{n}l}$, the oxygen mass fraction, has been monitored at the spheroid center during 4 days (see Fig ***Figure 10***) . The thinner mesh of cell size $dh = 2.5\,\mu$m has been used as reference for the RMSE. Despite an important increase of the computation time, the mesh of cell size $dh = 5\,\mu$m has been chosen to restrict the relative degradation of the FE solution to $RMSE = 0.01$ (see Table 2).

Verification of the FE formulation with an analytical solution

If this system is considered with a single phase flow into a porous medium under a constant load with the right boundary conditions, one obtains the problem as known as Terzaghi's consolidation, which has an analytical solution ***Verruijt*** (***2013***). The system, under a constant load $\mathbf{T}$, is reduced to two primary variables the displacement of the solid scaffold $\mathbf{u}^s$ and the pressure of the single phase fluid p^l:

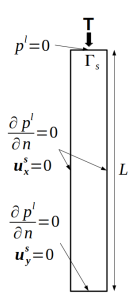

$$\begin{cases} \nabla.\mathbf{v}^s - \nabla.\left[\frac{k}{\mu}\nabla p^l\right] = 0 \text{ on } \Omega \\ \nabla.\bar{\bar{t}}_t = 0 \text{ on } \Omega \\ \nabla.\bar{\bar{t}}_t = -\mathbf{T} \text{ on } \Gamma_s \end{cases} \quad \text{with } \mathbf{T} = \begin{pmatrix} 0 \\ p_0 \end{pmatrix} \tag{29}$$

The fluid is free to escape only at the loaded boundary, this boundary condition is known as drying condition. The analytical solution of this problem is:

$$p^l(y,t) = p_0 \frac{4}{\pi} \sum_{k=1}^{\infty} \frac{(-1)^{k-1}}{2k-1} \cos\left((2k-1)\frac{\pi}{2}\frac{y}{L}\right) \exp\left((2k-1)^2 \frac{\pi^2}{4}\bar{t}\right) \tag{30}$$

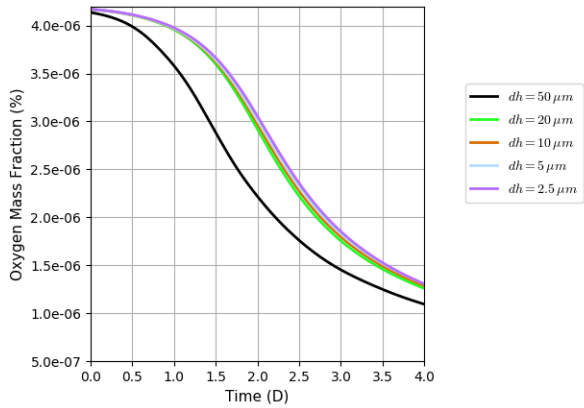

Appendix 0 Figure 10. Sensibility of the solution related to mesh refinement. The oxygen mass fraction, $\omega^{\bar{n}l}$, at the center of the spheroid has been monitored during six days for five different cell sizes. ($dh = 50\,\mu$m, black ; $dh = 20\,\mu$m, green ; $dh = 10\,\mu$m, brown; $dh = 5\,\mu$m, light blue ; $dh = 2.5\,\mu$m, purple)

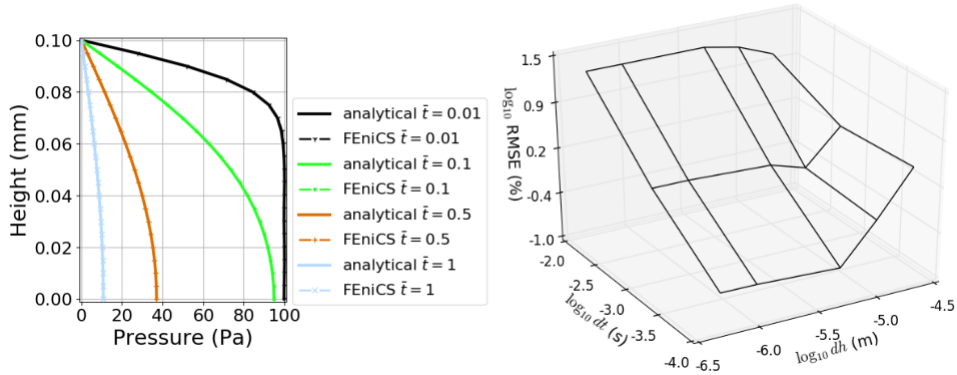

Appendix 0 Figure 11. Left: qualitative comparison between analytical solution of Terzaghi's problem and FEniCS computation. (4 comparisons at characteristic time of consolidation $\bar{t} = 0.01, 0.1, 0.5, 1$). Right: quantitative comparison: error surface between Terzaghi's analytical solution and FEniCS computation. (x axis: $\log_{10}$ of cell size dh ; y axis: $\log_{10}$ of dt ; z axis: $\log_{10}$ of RMSE). The minimum RMSE= 0.0028 is reached at $dh = 5\mu$m, $dt = 1e^{-4}$

With the characteristic time of the consolidation $\bar{t}$, equal to $\frac{c_v t}{L^2}$, L sets to $100\,\mu$m and c_v, the consolidation coefficient:

$$c_v = \frac{k}{\mu^l}(\lambda + 2\mu)$$

where λ and μ are Lamé constants of the solid scaffold, k is its intrinsic permeability and μ^l the fluid dynamic viscosity. The addition of the RMSE of the 4 samples at $\bar{t} = 0.01, 0.1, 0.5, 1$ (see Fig.***Figure 11***) with the analytical solution as reference gives $\sum RMSE = 0.0028$. The surface error for different cell sizes dh and time steps dt is in Fig.***Figure 11***(right).

Appendix C. Sensitivity analysis

The seven parameters of the model have been set to generic values, gathered Table 1 in the main article. The FE solutions with this values, at day 4 for the free MCTS and day 1 the encapsulated one, have been compared with the experimental results through cost functions, J_{free} and J_{conf}, defined below. We have chosen the following design of experiment (DOE): for each configuration, each parameter one at a time has been perturbed of $[-10, -5, -2, -1, +1, +2, +5, +10]\%$ and the corresponding cost has been computed (see ***Figure 12*** and ***Figure 13***).

Scaling of parameters

The seven parameters to optimize have a wide range of values from $6000\,[Pa]$ to $4.10^{-4}\,[kg/(m^3.s)]$. To analyse the influence of their gradient on the finite element solution, unit-norm auxiliary parameters have been considered:

$$\begin{pmatrix} \alpha_a & 0 & 0 & 0 & 0 & 0 & 0 \\ 0 & \alpha_{\mu_t} & 0 & 0 & 0 & 0 & 0 \\ 0 & 0 & \alpha_{\gamma_g^t} & 0 & 0 & 0 & 0 \\ 0 & 0 & 0 & \alpha_{\gamma_g^{nl}} & 0 & 0 & 0 \\ 0 & 0 & 0 & 0 & \alpha_{\gamma_0^{nl}} & 0 & 0 \\ 0 & 0 & 0 & 0 & 0 & \alpha_{p_1} & 0 \\ 0 & 0 & 0 & 0 & 0 & 0 & \alpha_{p_{\text{crit}}} \end{pmatrix} \begin{pmatrix} a \\ \mu_t \\ \gamma_g^t \\ \gamma_n^t \\ \gamma_g^{nl} \\ \gamma_0^{nl} \\ p_1 \\ p_{\text{crit}} \end{pmatrix}$$

With all the α_i set to 1. These parameters have been perturbed of $[-10, -5, -2, -1, +1, +2, +5, +10]\%$.

Cost functions

To study the cell-line specific parameters, the experimental data of the free MCTS have been used. However, the only physical quantity given for this configuration is the MCTS volume. This sparse experimental data in front of a multiphase system have made difficult to set a well defined cost function. To build a defined and differentiable one, a simulation noted Y_{goal} has been run freely until it reaches the experimental volume of days 1,2,3 and 4. At the corresponding iterations, the numerical quantities as porosity ε and tumor phase saturation S^t have been stored to be used has goal. For the day i, the tumor volume is equal to:

$$V_{\text{goal}_i} = \int_\Omega \varepsilon_i S_i^t \, dx$$

Where Ω is the whole computation domain, as $S^t = 0$ outside of the tumor zone.
Then a simulation with the same parameters, has been run for 4 days and its volume has been compared to Y_{goal} at the time steps corresponding to 1, 2, 3 and 4 days, noted $D_i\ (i = 1, 2, 3, 4)$. One can write this cost function explicitly:

$$J_{\text{free}}(X, \Phi) = \sum_{i=1}^{4} \int_\Omega \left[\varepsilon(D_i) S^t(D_i) - \varepsilon_i S_i^t\right]^2 \, dx \tag{31}$$

For the confinement configuration, the cost function $J_{conf}(X, \Phi)|_T$ has the classical form:

$$J_{\text{conf}}(X, \Phi)|_{T_i} = \int_{\partial_{\text{Caps}}} < F(X, \Phi, T) - Y(T) > \, ds$$

Where the observable Y has two components, Y_1 is the experimental measurement of the capsule displacement at time T_i after confluence, on ∂_{Caps}, which corresponds to the interface between the MCTS and the alginate capsule, and Y_2 the analytical pressure on capsule given in ***Alessandri et al.*** (***2013***). The numerical approximation $F(X, \Phi, T)$ has the two corresponding components $(\mathbf{u}^s, p^s)$ in $\partial_{\text{Capsule}}$. We compared the FE solution with the experimental data 1 day after confluence. One can write this cost function explicitly:

$$J_{\text{conf}}(X, \Phi)|_{\text{day 1}} = \int_{\partial_{\text{Caps}}} < u^{\text{exp}} - u^s > \, ds + \int_{\partial_{\text{Caps}}} (p^{\text{exp}} - p^s)^2 \, ds \tag{32}$$

Figure 12 and ***Figure 13*** show J_{free} and J_{conf} respectively, for the whole design of experiment. They are the magnification of the pie charts of the parameters sensitivity in the main article, thus we can see the details of the governing parameters of each configuration.

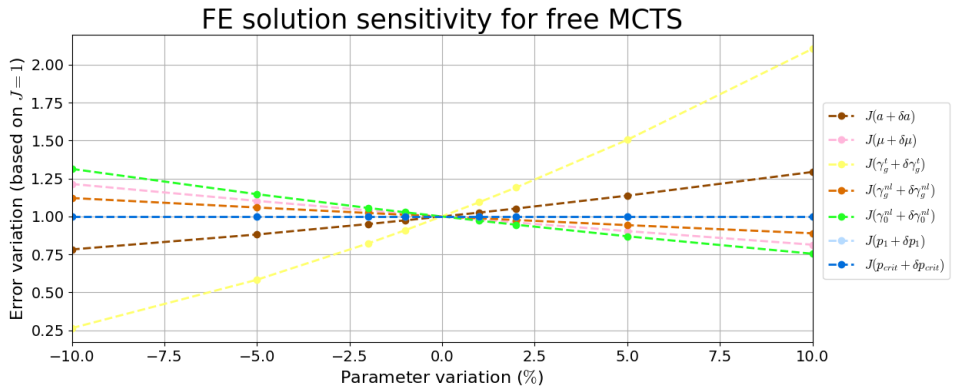

Appendix 0 Figure 12. Design of experiment (DOE) for the free MTCS. The seven parameters have been, one at a time, perturbed of $[-10, -5, -2, -1, +1, +2, +5, +10]\%$. The most sensitive parameter is clearly γ_g^t, the TC growth rate. The DOE has a global profile of linear sensitivity and for p_1 and p_{crit} the FE solution sensitivity is 0.

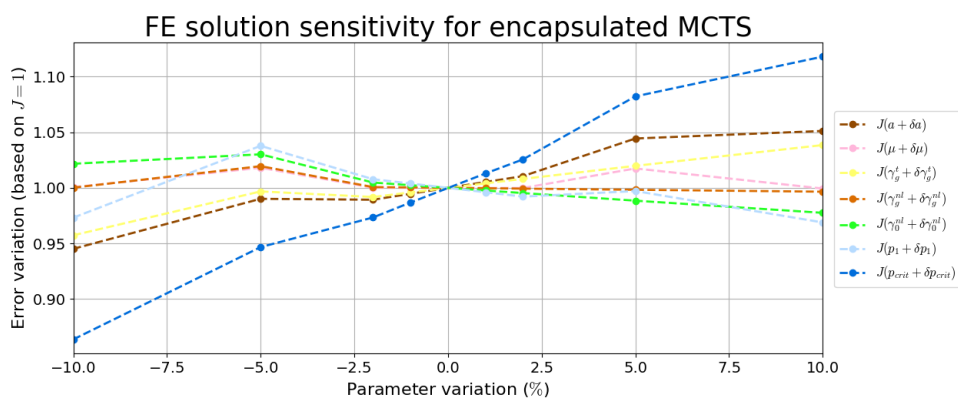

Appendix 0 Figure 13. Design of experiment (DOE) for the encapsulated MTCS. The seven parameters have been, one at a time, perturbed of $[-10, -5, -2, -1, +1, +2, +5, +10]\%$. The most sensitive parameter is clearly p_{crit}. The DOE shows an unstable sensitivity profile and non-convex for p_1, the first inhibitory pressure threshold.